nature geoscience

SUPPLEMENTARY INFORMATION

DOI: 10.1038/NGEO1111

Patterns of intraplate volcanism controlled by asthenospheric shear

Clinton P. Conrad[1,†,*], Todd A. Bianco[1,‡], Eugene I. Smith[2], and Paul Wessel[1]

[1] Department of Geology & Geophysics, School of Ocean and Earth Science and Technology, University of Hawaii at Manoa, Honolulu, HI 96822, USA
[2] Department of Geoscience, University of Nevada Las Vegas, Las Vegas, NV 89154, USA
[†] Currently visiting: Center for Advanced Studies, Norwegian Academy of Letters and Sciences, NO-0271, Oslo, Norway
[‡] Now at: Department of Geological Sciences, Brown University, Providence, RI 02912, USA
[*] Corresponding Author (clintc@hawaii.edu)

Magnitude of Asthenospheric Shear

We estimate the magnitude of shear in the asthenosphere using the global mantle flow model of *Conrad & Behn* [2010], who used a combination of mantle density heterogeneity, surface plate motions, and net lithosphere rotation to drive mantle flow, and constrained the relative importance of these components using observations of azimuthal seismic anisotropy. Although *Conrad & Behn* [2010] found that a range of possible mantle flow solutions fit the anisotropy data, we use their "preferred" best-fitting model, which assumes an upper mantle viscosity of 0.5×10^{20} Pa s, an asthenospheric viscosity 10 times smaller, lateral variations in lithospheric thickness defined by *Conrad & Lithgow-Bertelloni* [2006], relative plate motions consistent with the NUVEL-1A [*DeMets et al*., 1994] plate motion model, and net lithosphere rotation corresponding to 20% of the net rotation associated with the HS3 Pacific hotspot plate reference frame [*Gripp & Gordon*, 2002].

Although the parameters that control mantle density and viscosity structures, net lithosphere rotation, and cratonic thickness variations all influence the mantle flow field to some degree, the basic pattern of mantle flow for reasonable choices of these parameters is rather robust. For example, the asthenospheric flow field shown by *Conrad & Behn* [2010] is largely similar to the family of models presented by *Becker* [2006], who made different choices for all of the relevant parameters (e.g., compare Fig. 2 of *Becker* [2006] with Fig. 8 of *Conrad & Behn*

DOI: 10.1038/NGEO1111

[2010]). Probably the most important parameter for asthenospheric shear amplitude is the asthenospheric viscosity drop, without which shear amplitudes would be significantly smaller due to tight coupling between the upper mantle and the plate motions. The *Conrad & Behn* [2010] flow model used here assumes that the asthenosphere is 10 times less viscous than the upper mantle, which permits the concentrated shearing of the asthenosphere that is necessary to produce anisotropic structure. Larger viscosity drops, although possible, do not affect asthenospheric shear patterns significantly [*Conrad & Behn*, 2010].

To estimate the magnitude of asthenospheric shear from *Conrad & Behn's* [2010] model, we measured the magnitude of the vector difference between surface plate motion and the horizontal flow field at the base of the low-viscosity asthenosphere (300 km depth in *Conrad & Behn's* [2010] model, as estimated from laboratory experiments [e.g., *Karato & Wu*, 1993]) (Fig. S1). This quantity expresses surface plate motion in the (local) reference frame of the mantle at 300 km, and therefore quantifies the net shearing that occurs across the deforming asthenosphere.

Designation of Regions of Recent Intraplate Volcanism for Continental Areas

To designate the regions of the continents that have recently exhibited intraplate volcanism, we use the www.earthchem.org database and select all igneous rock types with a classification of "volcanic", "mafic", and " basalt". Because we want to consider only volcanic regions that were active for a mantle flow field similar to that estimated for the present-day, we limit our search to samples with measured ages less than 10 Ma, which is the approximate age of the most recent major reorganization of plate motions [*Gordon & Jurdy*, 1986; *Lithgow-Bertelloni & Richard*, 1998; *Müller et al.*, 2008]. This results in 8692 unique samples (Fig. S2), as accessed by www.earthchem.org from the GEOROC, NAVDAT, and USGS databases in June 2010. To exclude samples that are associated with plate boundary processes such as subduction or rifting, we remove samples whose locations are within 300 km of a continental rift, a continental convergent boundary, an oceanic spreading ridge, an oceanic convergent boundary, or a subduction zone, as defined by *Bird's* [2003] plate boundary model. We found that excluding samples that are clearly associated with hotspot volcanism, such as those that are within 300 km of one of the 9 major hotspots defined by *Courtillot et al.* [2003] (defined as

exhibiting at least 3 out of 5 diagnostic criteria; locations of the 9 hotspots are shown in Figs. 1A and 2A) in fact removed no additional continental samples. This is because samples from the single major continental hotspot (Afar) are already excluded because they lie within 300 km of a continental rift.

The above exclusions narrow the number of "intra-plate" volcanic samples to 3760 (dark green dots, Fig. 1A). Many of these samples access nearby rocks from the same volcanic field, and are therefore essentially duplicates for the purposes of delineating the location and expanse of intraplate volcanism. To eliminate these duplications, we determine which continental locations (on a 1 by 1 degree grid) lie within 100 km of the location of an "intraplate" volcanic sample (light green area, Fig. 1A insets). Thus, for each continental point that is at least 300 km from a volcanic plate boundary or hotspot (81.8% of the continental area), we have delineated the continental regions that have exhibited at least some intra-plate volcanism within the last 10 Myr (3.1% of continental area), and those that have not (78.7%). Note that the basaltic volcanism fields that are delineated by this method occur on all continents and exhibit areas ranging from single locations to regions more than ~1000 km wide (e.g., western North America). Despite this wide coverage, it will be difficult to assess whether spatial coverage of intraplate volcanism is complete until significant growth of the number of samples in the www.earthchem.org database fails to introduce new regions of intraplate volcanism.

Designation of Regions of Recent Intraplate Volcanism for Submarine Areas

To designate the regions of the ocean basins that have recently produced intraplate volcanism, we use *Wessel's* [2001] global survey of seamounts, which provides locations and sizes for 11,882 seamounts distributed across the seafloor (Fig. 2A). This database provides globally-uniform coverage, but only contains seamounts large enough (>1.5 km in height) to be well resolved by satellite altimetry. Smaller seamounts, despite being more numerous and the most obvious candidates for shear-driven volcanism, are not included in the study because they can only be detected from ship track bathymetry, which does not cover the seafloor uniformly. We note, however, that the distribution of larger seamounts has been observed to be similar to, and even predictive of, the distribution of smaller seamounts [*Hillier & Watts*, 2007].

We re-computed seafloor ages for *Wessel's* [2001] seamounts using the recent *Müller et*

DOI: 10.1038/NGEO1111

al. [2008] age grid. To obtain statistics for seamounts that formed recently (and for which we can estimate asthenospheric shear magnitude using *Conrad & Behn's* [2010] global mantle flow model), we considered only the 558 seamounts that reside on seafloor that is less than 10 Myr old (Fig. 2A). Many of these near-ridge seamounts are located along the western side of the East Pacific Rise (EPR) (Fig. 2A, inset), but also occur along the South-East Indian Ridge, Southern Mid-Atlantic Ridge, Juan de Fuca Ridge, and on the eastern side of the EPR (Fig. 2A). Following the same method that we used to designate regions of continental volcanism, we determine which regions of young (ages <10 Ma) seafloor (on a 1 by 1 degree grid) lie within 100 km of one of these 558 young seamounts (Fig. 2A inset, light blue area).

Time Dependence of Seamount Emplacement

Because direct measurement of seamount ages is infeasible, several authors have used observations of vertical gravity gradient amplitudes [e.g., *Wessel*, 1997] or the elastic deflection of the seafloor to estimate the age of the seafloor at the time a seamount was emplaced [e.g., *Watts et al.,* 2006; *Hillier*, 2007]. Although significant uncertainty accompanies such age estimates for individual seamounts, this uncertainty is reduced in an average sense for groups of seamounts considered in aggregate. We used *Hillier's* [2007] estimates of seafloor age at the time of emplacement to group the 2706 seamounts in that study into those that formed near the ridge axis (on seafloor 0-10 or 10-20 Myr old), and those that formed on older seafloor (20-45 or >45 Myr old) (Fig. S5). We removed seamounts with volumes larger than 10^4 km^3 from the *Hillier* [2007] database because these large seamounts are readily explained by hotspot volcanism (e.g., Hawaii). For each group, we computed the total seamount volume emplaced on the seafloor using 10 Myr running seafloor age windows (seafloor age was computed for each seamount using the *Müller et al.* [2008] age grid). To estimate the average seamount volume density as a function of time on the Pacific seafloor, we divided these volumes by the total present-day area of seafloor within the same 10 Myr seafloor age windows (Fig. 3). Note that the uncertainty in the age estimation for individual seamounts is apparent in the presence of small seamount volumes with seafloor emplacement ages that are younger than the seafloor on which these seamounts reside (Fig. 3).

References Cited in Supplementary Materials

Becker, T. W. On the effect of temperature and strain-rate dependent viscosity on global mantle flow, net rotation, and plate-driving forces. *Geophys. J. Int.* ***167*****,** 943-957 (2006).

Bird, P. An updated digital model of plate boundaries. *Geochem. Geophys. Geosys.* ***4*****,** 1027 (2003).

Conrad, C. P. & Behn, M. D. Constraints on lithosphere net rotation and asthenospheric viscosity from global mantle flow models and seismic anisotropy. *Geochem. Geophys. Geosys.* **11,** Q05W05 (2010).

Conrad, C. P. & Lithgow-Bertelloni, C. Influence of continental roots and asthenosphere on plate-mantle coupling. *Geophys. Res. Lett.* **33,** L05312 (2006).

Courtillot, V., Davaille, A., Besse, J. & Stock, J., Three distinct types of hotspots in the Earth's mantle. *Earth Planet. Sci. Lett.* **205,** 295-308 (2003).

DeMets, C., Gordon, R.G., Argus, D.F. & Stein, S. Current plate motions. *Geophys. J. Int.* **101,** 425-478 (1994).

Gordon, R.G. & Jurdy, D.M. Cenozoic global plate motions. *J. Geophys. Res.* **91,** 12389-12406 (1986).

Gripp, A. E. & Gordon, R. G. Young tracks of hotspots and current plate velocities. *Geophys. J. Int.* **150,** 321-361 (2002).

Hillier, J. K., Pacific seamount volcanism in space and time. *Geophys. J. Int.* **168,** 877-889 (2007).

Hillier, J. K. & Watts, A. B. Global distribution of seamounts from ship-track bathymetry data. *Geophys. Res. Lett.* **34,** L13304, (2007).

Karato, S.-i., & Wu, P. Rheology of the upper mantle: A synthesis. *Science* **260,** 771-778 (1993).

Lithgow-Bertelloni, C. & Richards, M.A., The dynamics of Cenozoic and Mesozoic plate motions, *Rev. Geophys.* **26,** 27-78 (1998).

Miles, R. E. On random rotations in R^3. *Biometrika* **52,** 636-639, 1965.

Müller, R.D., Sdrolias, M., Gaina, C. & Roest, W. R. Age, spreading rates, and spreading asymmetry of the world's ocean crust. *Geochem. Geophys. Geosyst.* **9,** Q04006 (2008).

Press, W. H., Flannery, B. P., Teukolsky, S. A., Vetterling, W. T. Numerical Recipes in Fortran. (Cambridge Univ. Press, New York, 1992).

Schervish, M. J. P Values: What they are and what they are not. *Amer. Stat.* **50,** 203-206 (1996).

Watts, A. B., Sandwell, D. T., Smith, W. H. F. & Wessel, P. Global gravity, bathymetry, and the distribution of submarine volcanism through space and time. *J. Geophys. Res.* **111,** B08408 (2006).

Wessel, P. Sizes and ages of seamounts using remote sensing: Implications for intraplate volcanism. *Science* **277,** 802-805 (1997).

Wessel, P. Global distribution of seamounts inferred from gridded Geosat/ERS-1 altimetry. *J. Geophys. Res.* **106,** 19431-19441 (2001).

DOI: 10.1038/NGEO1111

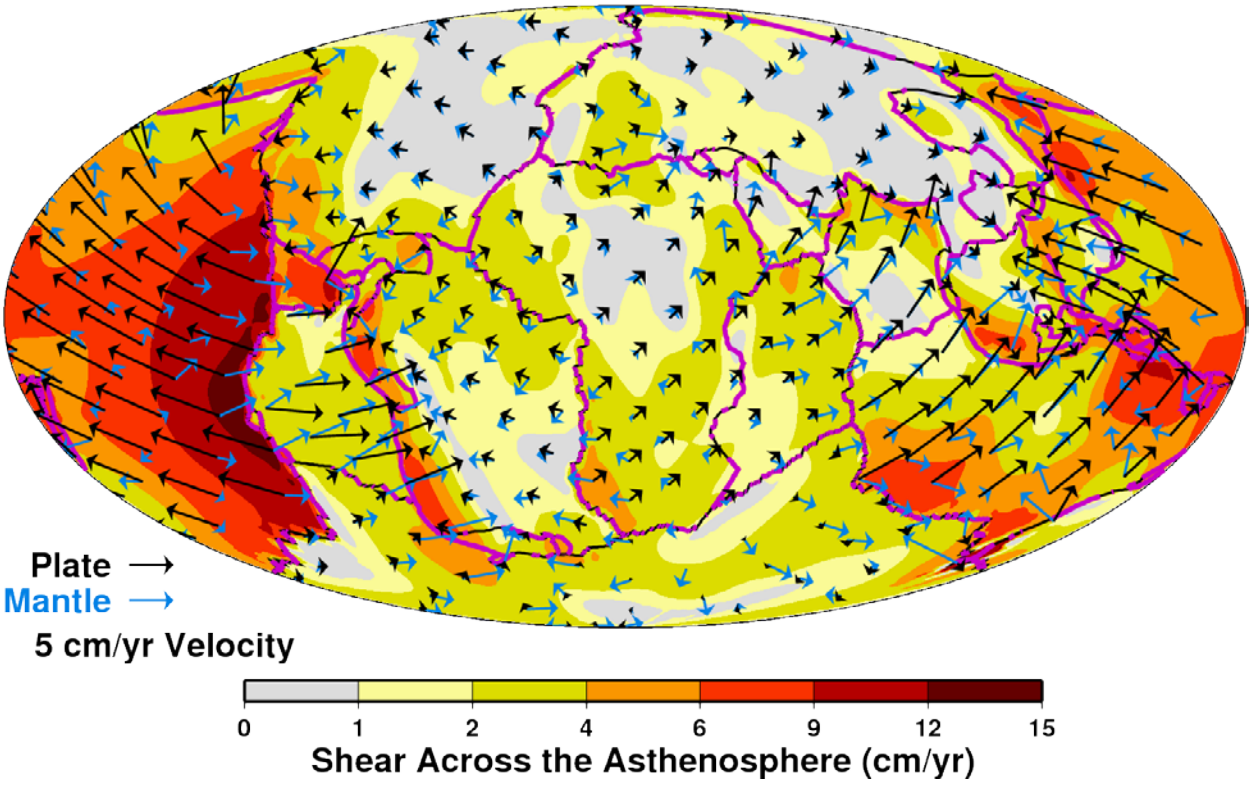

Figure S1. Global map of asthenospheric shear magnitudes. Shown are surface plate motions (0 km depth, black vectors), mantle flow at the asthenospheric base (300 km depth, blue vectors), and the magnitude of their vector difference (background colors), which is the amplitude of the shear deformation occurring across the asthenosphere. Flow field is based on the *Conrad & Behn* [2010] model for global mantle flow. Volcanic and non-volcanic plate boundaries (pink and black lines, respectively; the former include rifting and subducting plate boundaries from *Bird* [2003]) are shown for reference.

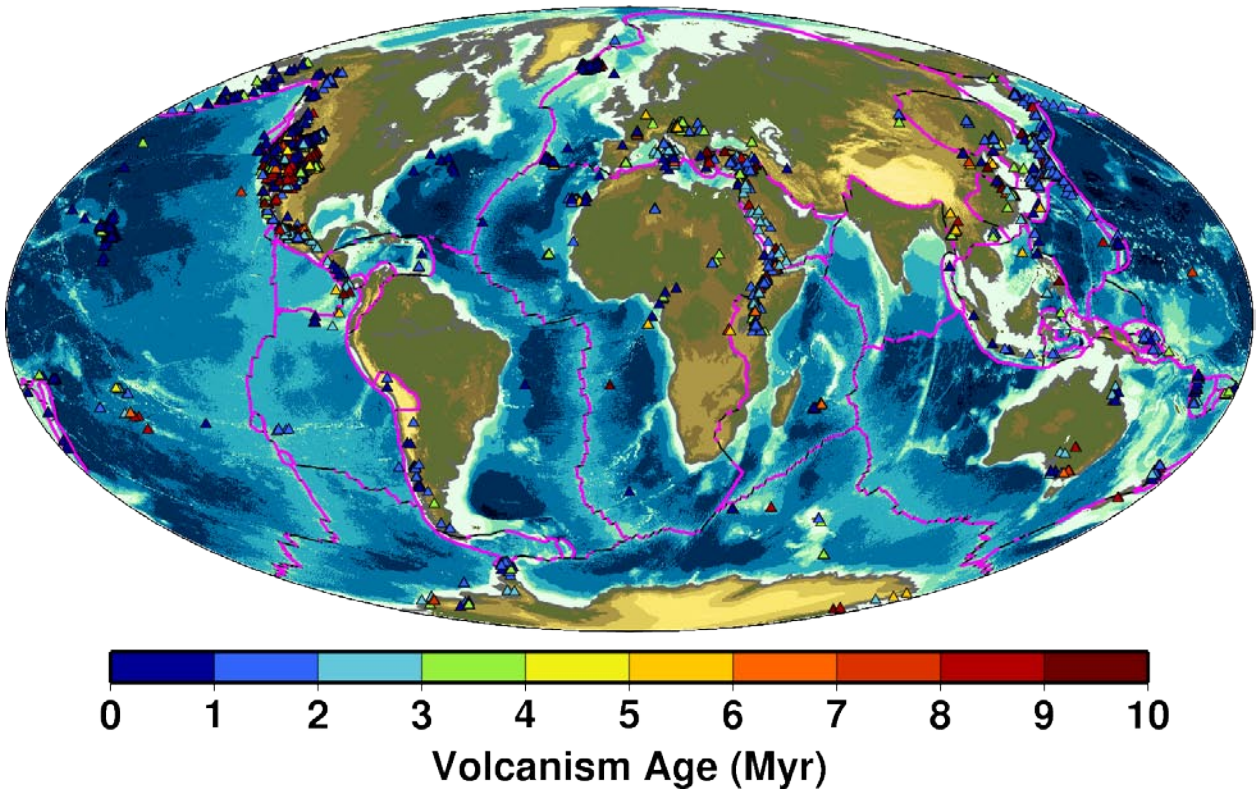

Figure S2. Locations of recent basaltic volcanism on earth. Volcanism locations are inferred from samples listed in the www.earthchem.org geochemical database that are classified as igneous, volcanic, mafic, and basaltic, and with ages less than 10 Ma (age is shown in colors). Volcanic and non-volcanic plate boundaries are shown as in Fig. S1.

DOI: 10.1038/NGEO1111

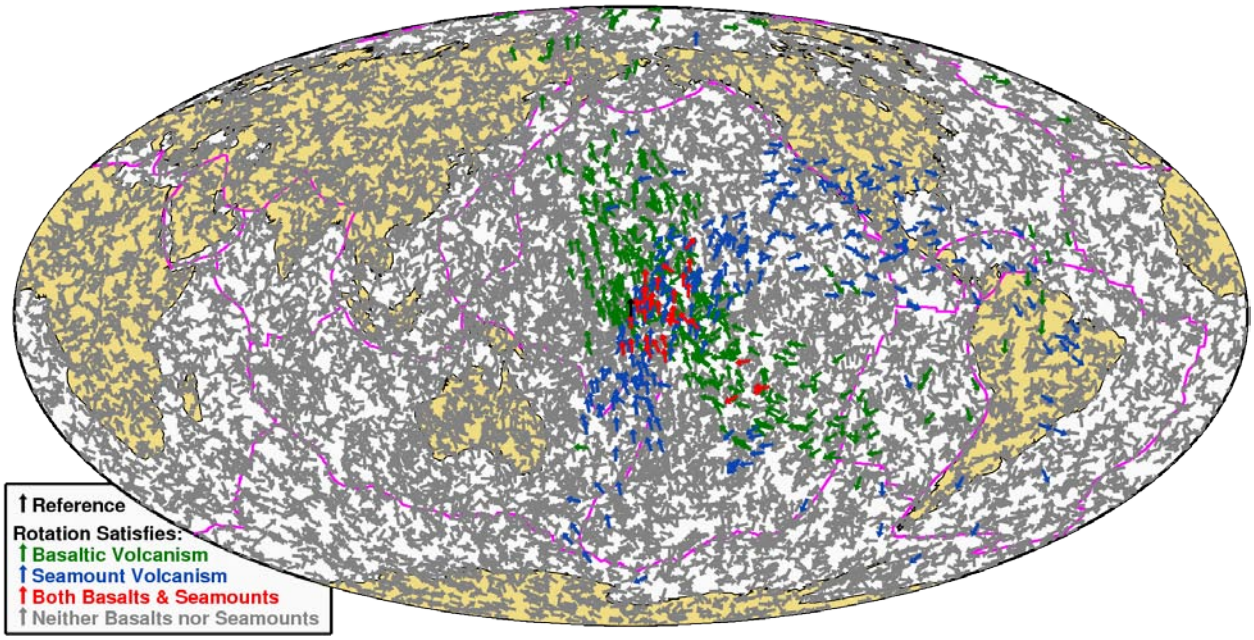

Figure S3. Random re-orientations of the asthenospheric shear pattern used to compute the p-value statistic. To re-orient the asthenospheric shear pattern into a new randomly-chosen position, we performed uniformly-distributed random rotations on the present-day asthenospheric shear pattern (Fig. S1). To ensure a uniform distribution of rotations, we follow *Miles* [1965] and picked rotation poles from a uniform distribution of points on the Earth's surface and rotation angles θ from the distribution $(\theta - \sin\theta)/\pi$, where $0 \leq \theta \leq \pi$. To compute p-values [e.g., *Schervish*, 1996], we performed 10,000 rotations, which can be visualized by the translation of a reference arrow (e.g., black arrow oriented northward in the middle of the Pacific) into one of 10,000 new orientations on the Earth's surface (non-black arrows). The 375 green arrows, 276 blue arrows, and 34 red arrows indicate orientations that contribute to the p-value statistic for continental intraplate volcanism, seamount volcanism, and both continental and seafloor volcanism simultaneously (respectively). Grey arrows indicate orientations that produce statistics that do not exceed the threshold of contributing to the p-value for either continental or seamount volcanism (see Methods).

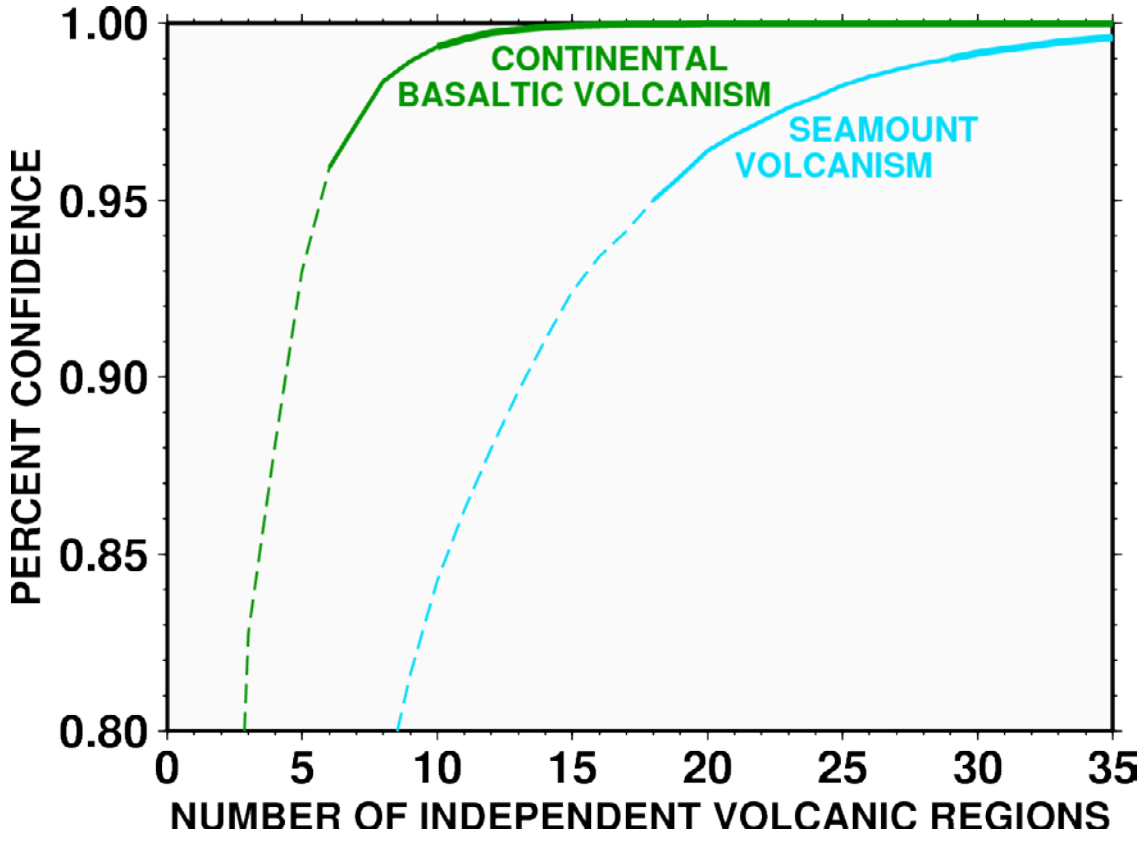

Figure S4. Confidence that the observed shear distributions for volcanism do not result from random sampling of the background shear distribution, as a function of the assumed number of independent volcanic regions. Confidence is estimated by applying the Kolmogorov-Smirnov test (see Methods and *Press et al.*, 1992) to pairs of distributions for continental regions (Fig. 1B) and young seafloor (Fig. 2B) (green and blue curves, respectively). Dashed line shows confidence level, and is replaced by a solid line if it rises above 95% and by a thick solid line if it rises above 99%.

DOI: 10.1038/NGEO1111

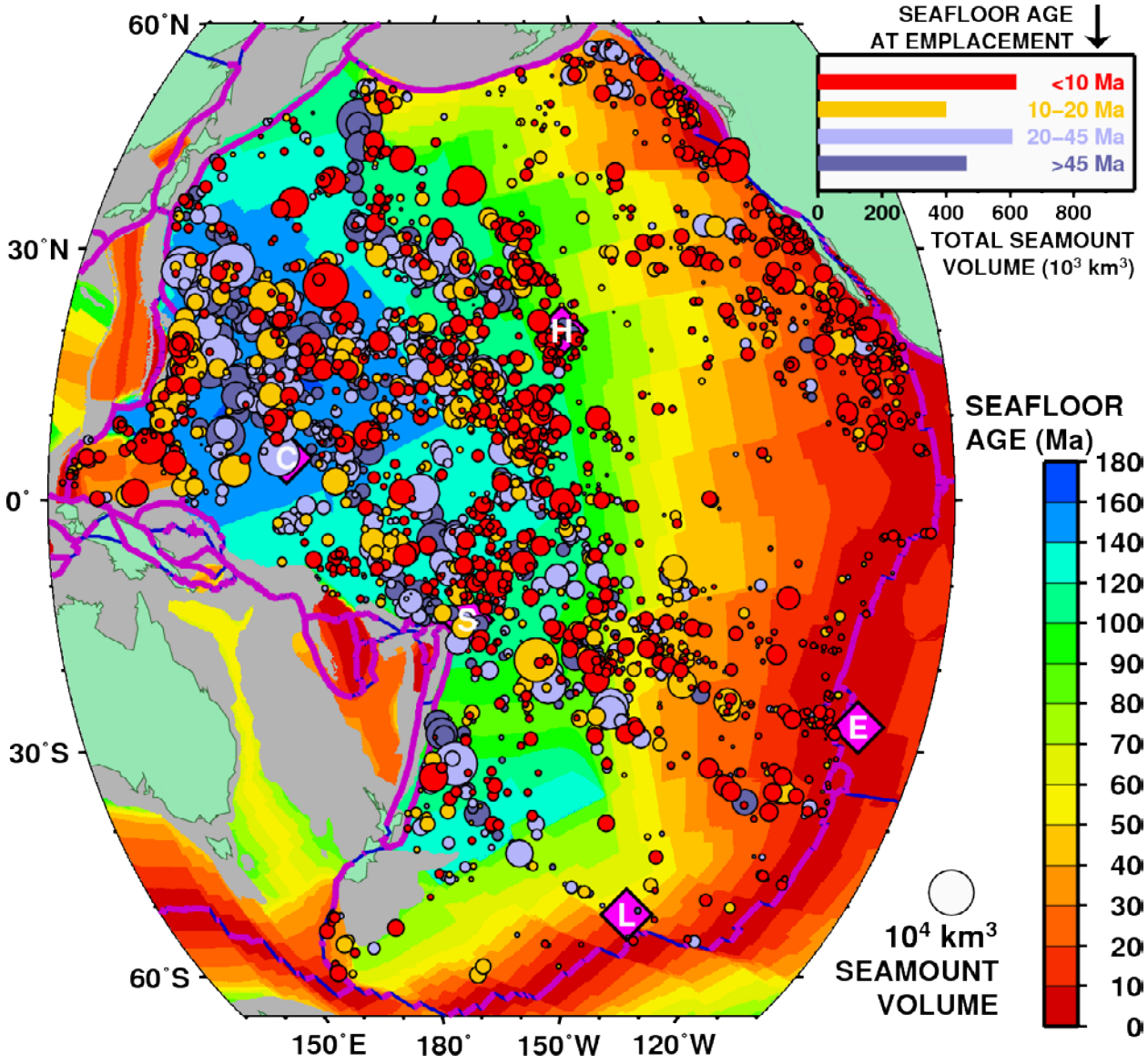

Figure S5. Seamount locations (circles) and volumes (area of circles) for the *Hillier* [2007] database of Pacific seamounts. Background colors show the current seafloor age, and circle colors show *Hillier's* [2007] estimates of seafloor age at the time each seamount was emplaced, with age ranges corresponding to those shown in the legend and in Fig. 3. Seamounts larger than 10^4 km^3 are removed from the database (see text).